

Letter

# Study on the edge isolation of industrial silicon solar cells with waterjet-guided laser

Daniel Kray<sup>a,\*</sup>, Sybille Hopman<sup>a</sup>, Akos Spiegel<sup>b</sup>, Bernold Richerzhagen<sup>b</sup>, Gerhard P. Willeke<sup>a</sup>

<sup>a</sup>Fraunhofer Institute for Solar Energy Systems (ISE), Heidenhofstr. 2, D-79110 Freiburg, Germany

<sup>b</sup>Synova S.A., Chemin de la Dent D'Oche, 1024 Ecublens, Switzerland

Received 22 February 2007; received in revised form 15 May 2007; accepted 15 May 2007

Available online 10 July 2007

## Abstract

In this paper, we review the device physics to explain the necessity of edge isolation as well as the various common methods for performing this important step. In order to assess these processes, different aspects have to be taken into consideration and will be discussed. Finally, experimental results of edge isolation on commercial multicrystalline solar cells with waterjet-guided laser (wavelength 1064 nm) and conventional laser (wavelength 355 nm) are presented and discussed. From the experiments, we conclude that the waterjet-guided laser shows the potential to improve the laser scribing process in terms of pn junction damage and mechanical stability.

© 2007 Elsevier B.V. All rights reserved.

**Keywords:** Edge isolation; Laser; Solar cells

## 1. Introduction

Unless the parasitic emitter diffusion wrapping around the wafer edge is removed, most industrial cells suffer from very low fill factors. This edge isolation process can be performed by different methods. Until a few years ago, plasma barrel etching was the standard process for edge isolation of solar cells. Since this batch process led to a strong disruption in the flow of the process due to stacking and unstacking of several hundreds of wafers, there was great interest in replacing this step by an appropriate inline process. One of the most successful new edge isolation processes is laser scribing. It is perfectly suitable for inline processing and the wafer needs not to be touched, which is an important requirement for the handling of thin wafers. In these systems, mostly solid-state lasers like Nd:YAG with short wavelengths (e.g., frequency tripled with  $\lambda = 355$  nm) are used. Even though the absorption of silicon in this wavelength range is very good and the pulses are quite short, the results are not always satisfying due to the recast of molten or evaporated silicon with respective

mechanical stresses in the wafers or focusing problems with wafers of inhomogeneous thickness.

Therefore, alternatives to the conventional laser edge isolation have to be assessed if the commercial performance of the edge isolation step is to be further increased. An emerging new laser process that has the potential to overcome the problems of conventional lasers is the waterjet-guided laser [1,2] which has been studied experimentally in the present work.

An interesting option is the performance of edge isolation on the rear side of the cell because this prevents the damaging of the front side emitter where most of the photogeneration takes place. The difference between front and rear side edge isolation has been investigated experimentally as well as by DESSIS simulations.

### 1.1. Why do commercial solar cells need edge isolation?

Fig. 1 shows a sketch of a commercial screen-printed solar cell design. In the standard processing sequence, the entire wafer is phosphorous diffused. The contact to the p-type base is made by firing an Al containing paste that produces a local high doping of Al, thus overcompensating the shallow emitter diffusion. However, there is still a direct

\*Corresponding author. Tel.: +49 761 4588 5355;  
fax: +49 761 4588 9250.

E-mail address: [daniel.kray@ise.fraunhofer.de](mailto:daniel.kray@ise.fraunhofer.de) (D. Kray).

conductive path from the emitter on the front side to the rear p-contact. Therefore, a large portion of the photo-generated current can directly flow through the emitter to the back contact instead of flowing through the external circuit. This current path is modeled in the two-diode model of the solar cell as the parallel resistance  $R_p$ :

$$j(V) = j_{01} \left( \exp \frac{V - jR_s}{n_1 V_{th}} - 1 \right) + j_{02} \left( \exp \frac{V - jR_s}{n_2 V_{th}} - 1 \right) + \frac{V - jR_s}{R_p} - j_L.$$

In this equation  $j_{01}$  and  $j_{02}$  represent the first and second diode saturation current densities;  $R_s$  and  $R_p$  are the series and parallel resistances, respectively;  $n_1$  and  $n_2$  denote the first and second diode ideality factors,

respectively;  $V_{th} = kT/q$  is the thermal voltage and  $j_L$  is the light-generated current density. In this model, the first diode accounts for emitter and bulk recombination with a recombination rate assumed to be proportional to the excess carrier density. This leads to an ideality factor of  $n_1 = 1$ . The second diode is associated with the recombination in the space-charge region that is assumed to be independent of the injection level, thus leading to  $n_2 = 2$ . The effect of increased  $j_{02}$  and  $R_p$  can be shown by model calculations for ideal solar cells in Fig. 2: for a fill factor above 84%,  $j_{02}$  must be less than  $2 \times 10^{-9} \text{ A/cm}^2$  and  $R_p$  must be greater than approximately  $2000 \text{ } \Omega \text{ cm}^2$  if the respective parameters contribute solely to the fill factor loss. This increase in  $R_p$  is achieved by the edge isolation process that interrupts the parasitic current path as shown in Fig. 1.

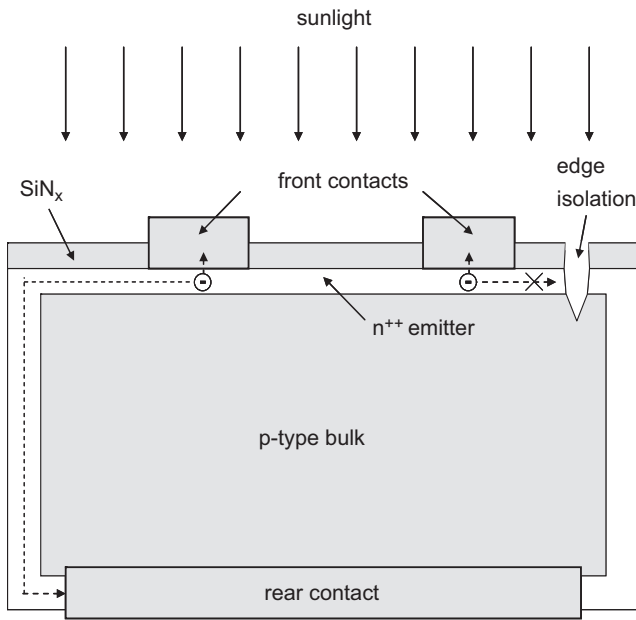


Fig. 1. Sketch of an industrial screen-printed solar cell. The emitter diffusion is present on the complete wafer surface and gets locally overcompensated by printing and firing an Al-containing metal paste as back contact. Without edge isolation, light-generated electrons can easily flow through the emitter region to the back contact which corresponds to a small series resistance in the two-diode model.

### 1.2. Common edge isolation methods

There are many different methods for performing edge isolation on silicon solar cells. These have been compared already by other authors [3–5]. The following processes are well known from the literature:

- plasma barrel etching [5],
- conventional laser grooving [5–7],
- dry etching [8],
- inline wet etching [3], and
- dispensing of etching pastes [9].

A general agreement exists that the interruption of the process flow associated with the plasma barrel etching is very disadvantageous. The laser and etching processes each have specific advantages and disadvantages. In this paper, laser and wet etching will not be compared in detail, despite the fact that both obtained an important market share, but it will be examined, whether the quality of the laser processing can be improved by guiding it in a thin waterjet.

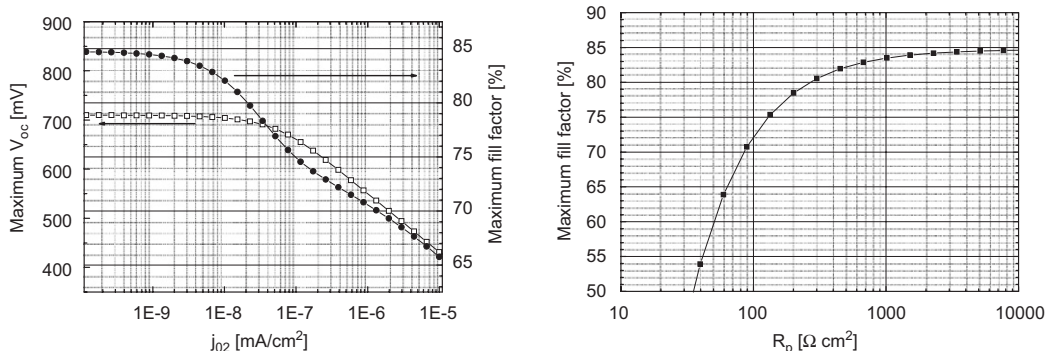


Fig. 2. Two-diode model calculations showing the fill factor and  $V_{oc}$  limitations imposed by  $j_{02}$  (left) and  $R_p$  (right). The respective assumptions were  $n_1 = 1$ ,  $n_2 = 2$ ,  $j_L = 42 \text{ mA/cm}^2$ ,  $j_{01} = 5 \cdot 10^{-14} \text{ A/cm}^2$ ,  $R_s = 0 \text{ } \Omega \text{ cm}^2$ ,  $R_p = 10^{10} \text{ } \Omega \text{ cm}^2$  (left) and  $j_{02} = 10^{-18} \text{ A/cm}^2$  (right).

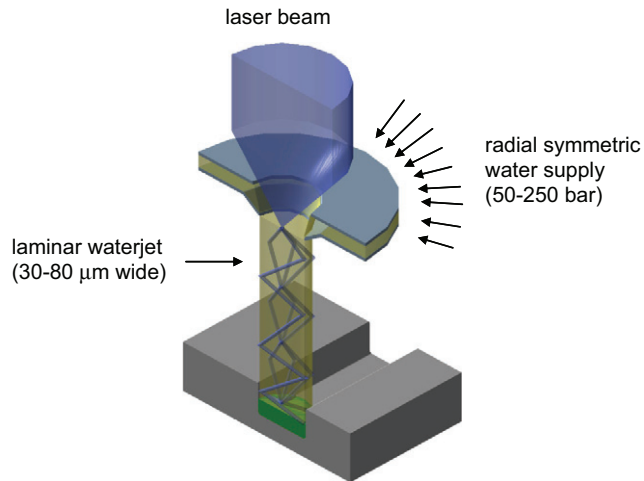


Fig. 3. Principle of the waterjet-guided laser. A hair-thin waterjet is generated in a flat nozzle with a glass window on top. A laser beam is focussed through this window into the waterjet thus allowing for guiding the laser beam just like in a liquid fiber.

### 1.3. Comparison of ‘dry’ and ‘waterjet-guided’ laser edge isolation

A sketch of the waterjet-guided laser is depicted in Fig. 3. A hair-thin waterjet (diameter down to 30  $\mu\text{m}$ ) is generated and the laser beam is focused into the jet through a transparent window on top of the water nozzle. The laser is guided via internal total reflection in the waterjet. This leads to a constant laser spot size independent of the distance between nozzle and wafer thus eliminating the need of refocusing if the wafer thickness changes. Additionally, the waterjet with its high flow velocity of up to 200 m/s can efficiently cool the groove after laser melting or evaporation and carry away the debris that generate unwanted recast in conventional laser processing. The waterjet-guided laser has already shown excellent performance in several microelectronic applications [10,11].

In order to assess whether the microstructuring quality of the waterjet-guided laser can also improve the edge isolation process for silicon solar cells, an experimental study with commercial solar cells was performed. Since the guidance of the laser in the waterjet increases the process complexity slightly compared to dry lasers, the edge isolation process must definitively be improved in terms of electrical and/or mechanical quality. If no other wet process follows the edge isolation, an additional drying step is necessary. However, there are also ideas how to reduce the effort for wafer drying considerably.

## 2. Experimental procedure

One hundred and twenty-five multicrystalline industrial solar cells of  $156 \times 156 \text{ mm}^2$  size were purchased of which 95 were not yet edge isolated. Preliminary tests on 15 cells were performed to optimize the laser parameters for the waterjet-guided laser. The main focus was to achieve

comparable groove depths with different parameters and to determine the minimum depth to ensure electrical isolation of the cells. The chosen laser parameter variations that have been used to isolate 70 solar cells (at 300  $\mu\text{m}$  distance from the edge) are summarized in Table 1. Those yielded different cutting depths with different scanning speeds and pulse frequencies and have been applied to front and rear side. The pulse overlap was chosen to be close to or above 80% according to the results of Emanuel et al. [6]. It should be noted that due to technical problems, only straight lines have been grooved with the waterjet-guided laser, leaving the beveled corners without isolation. This would of course be possible with a commercial system with optimized laser and motion control.

As a first reference, a laser edge isolation process with a dry laser ( $\lambda = 355 \text{ nm}$ ) with flying optics was applied to 10 cells while the distance of the groove to the edge was 250  $\mu\text{m}$ . The exact parameters of the manufacturer’s laser edge isolation, which were used as a second reference, are not known but the measured groove depth was about 10  $\mu\text{m}$ , comparable to our UV dry laser process.

The dark and illuminated *IV* curves have been measured before and after edge isolation. Additionally, dark thermography maps with forward and reverse voltage [12] were recorded for cells with typical performance to detect ohmic and non-ohmic edge shunts. To exclude the influence of the series resistance losses,  $S_{\text{uns}}-V_{\text{oc}}$  measurements [13] were performed for these cells as well. Finally, microscope observations (light microscope and SEM) as well as four line-breaking tests [14] have been performed which tests especially the mechanical quality of the wafer edges.

## 3. Results

### 3.1. *IV* curves measurements

In Table 2, the illuminated *IV* parameters are shown for the different processes. It can be seen that the waterjet-guided laser can reach results comparable to the dry lasers. This was accomplished with nearly industrial scanning speeds of 250 mm/s that could be further increased to about 500–600 mm/s by faster wafer stages. Only for the 5- $\mu\text{m}$ -deep grooves (variants 3, 4, 7, 8), a low fill factor is observed. For the variants with fill factors above 70%, values of  $R_{\text{p}}$  between 2 and 7  $\text{k}\Omega\text{cm}^2$  could be fitted.

This is a very positive result since the waterjet-guided laser system used in the process suffered from the following three drawbacks compared to the dry lasers:

- (1) An IR laser source was used that decreases the absorption coefficient in silicon by five orders of magnitude compared to the UV wavelength. Therefore the heat-affected zone is considerably larger.
- (2) The beveled corners of the cells were not isolated due to technical problems.
- (3) A 100- $\mu\text{m}$  nozzle was used, generating a groove width of about 80  $\mu\text{m}$  that corresponds to two to three times

Table 1  
Parameter variation for edge isolation with waterjet-guided laser

Variant no.	Laser power (W)	Pulse repetition rate (kHz)	Scanning speed (mm/s)	Pulse overlap (%)	Structured surface	Laser groove depth ( $\mu\text{m}$ )
1	40.4	13	250	77	Front side	20
2	40.4	13	250	77	Rear side	20
3	22.8	13	250	77	Front side	5
4	22.8	13	250	77	Rear side	5
5	45.2	20	250	85	Front side	20
6	45.2	20	250	85	Rear side	20
7	23.9	20	250	85	Front side	5
8	23.9	20	250	85	Rear side	5
9	40.4	13	100	90	Front side	40
10	45.2	20	100	94	Front side	45

A fiber-coupled Spectron Nd:YAG laser system with pulse length in the order of several hundreds of ns was used for the study. The water pressure was set to 100 bar and a nozzle with 100- $\mu\text{m}$  diameter was used. Since the laser power was measured after the fiber, the optical losses in the waterjet and the coupling unit are not taken into account.

Table 2  
Effect on fill factor,  $j_{\text{sc}}$  and efficiency of industrial multicrystalline solar cells of  $156 \times 156 \text{ mm}^2$  size after different edge isolation processes compared to the solar cells without edge isolation

Variant no.	Average fill factor, FF	Average fill factor improvement, $\Delta\text{FF}$ (% <sub>rel</sub> )	S.D. of $\Delta\text{FF}$ (%)	Average $J_{\text{sc}}$ ( $\text{mA}/\text{cm}^2$ )	Average efficiency improvement (% <sub>rel</sub> )	No. of measured solar cells
1	0.751	+20.0	1.6	31.5	+22.0	7
2	0.747	+19.4	1.2	31.8	+23.3	7
3	0.688	+10.1	1.5	31.6	+11.4	7
4	0.678	+8.5	1.4	31.4	+9.8	7
5	0.760	+22.1	1.4	31.5	+24.0	7
6	0.744	+18.5	1.1	32.5	+21.8	7
7	0.672	+6.8	1.2	32.1	+7.2	7
8	0.652	+3.7	0.8	32.0	+4.4	7
9	0.751	+19.7	2.0	32.0	+22.1	7
10	0.748	+19.2	1.3	32.2	+21.3	7
Dry UV laser	0.750	+19.8	1.6	31.9	+22.3	10
Industry reference	0.755			31.8		30

FF,  $\Delta\text{FF}$ ,  $J_{\text{sc}}$  and efficiency are average values. Variants 1–10 are the waterjet-guided laser processes described in detail in Table 1.

the groove width of the dry lasers. The front side areas outside the laser grooves as well as the laser-scribed areas have much lower quantum efficiencies than the rest of the solar cell. This is due to the laser damage and leads to a reduction in  $j_{\text{sc}}$  and  $V_{\text{oc}}$ .<sup>1</sup>

This fact gives rise to an optimistic outlook for experiments with waterjet-guided UV lasers that allows round corner isolation grooves and uses, e.g., 40- $\mu\text{m}$  nozzles.

Interestingly, the dark  $IV$  curves of all the cells isolated by the waterjet-guided laser showed a nearly perfect fit to the two-diode model with  $n_1 = 1$  and  $n_2 = 2$  while the cells isolated by the dry lasers could only be fitted with  $n_2 = 2.8$

<sup>1</sup>To observe this small effect clearly experimentally, larger amounts of cells have to be tested.

(average of 30 cells). This indicates that the removal of the molten silicon by the waterjet decreases the damage in the pn junction region.

### 3.2. Rear side edge isolation quality

It was also possible to perform rear side edge isolation for the studied cells. Schneiderlöchner reported in Ref. [15] the results for dry laser edge isolation experiments on solar cells from different manufacturers. Since the rear side isolation was equivalent to the front side isolation for only one material, he conjectured that edge defects, possibly from the brick cutting process, were not completely removed from the wafer edges for the material that did not allow rear side isolation.

To elucidate this problem, we performed 2D DESSIS simulations for a high-efficiency solar cell structure. In the

first case, the emitter wraps around the edge but does not reach the back contact (this represents an ideal rear side isolation). In the second case, the emitter is interrupted on the front side by a 50- $\mu\text{m}$  wide, passivated gap at 10  $\mu\text{m}$  distance from the edge (this is nearly an ideal front side isolation). The simulated illuminated cell parameters are shown in Table 3. Obviously, no edge defects are necessary to reduce the fill factor for the rear side isolation. This is simply done by the edge emitter that has a much lower injection level than the front emitter and is connected in parallel to the front emitter.  $V_{\text{oc}}$  is decreased by 10 mV and the fill factor is reduced by 2.5%<sub>abs</sub> compared to the front side isolation due to the higher recombination in this ‘dark’ emitter. More details about this issue will be published elsewhere.

However, in the DESSIS simulation, a current gain of more than 4% is assumed for the rear side isolation. In large industrial cells, this will not be realized. When the laser groove can be restricted to the area at a maximum distance of 300 (150)  $\mu\text{m}$  from the 156-mm-long cell edge, the ‘blinded’ area fraction is only 0.8 (0.4)%. A current gain in this order of magnitude does not compensate for

the fill factor and  $V_{\text{oc}}$  loss, so isolating from the front side seems to be the better process.

This is also true for our study: comparing the mean performance parameters of the cells with 20- $\mu\text{m}$  deep grooves (variants 1, 2, 5, 6 in Table 1), the cells isolated from the front side show nearly identical  $V_{\text{oc}}$  (1.4 mV less), lower  $j_{\text{sc}}$  (0.7 mA/cm<sup>2</sup> less) and higher fill factors (1.2%<sub>abs</sub>) than those isolated from the rear side. This leads to an increase in efficiency by 23.0%<sub>rel</sub> via front side edge isolation compared to 22.6%<sub>rel</sub> via rear side edge isolation.

### 3.3. Thermography maps

In Fig. 4, thermography maps at  $V_{\text{oc}}$  conditions are shown for the industrial reference, the waterjet-guided laser (variant 1 in Table 1) and the dry UV laser reference. It is to be noted that the edge areas between the busbars are obscured in the measurement setup so that no shunts are visible. Comparing the maps with the reverse bias measurements (not shown here) reveals that the right edge on the picture shows areas with ohmic shunting behavior for the dry laser processes while the other edges exhibit mostly diode-type behavior. The thermography maps of the cells isolated by the waterjet-guided laser show less recombination activity and a more homogeneous edge contrast compared to those from the cells scribed by the dry lasers. The homogeneous edge contrast indicates that the process fluctuations are less than for the other two laser scribing processes. Only the four unisolated corners are well visible in the map of the waterjet-guided laser. The shunts in the middle of two of the cells were introduced by problems with the contact probes in the  $IV$  measurements.

Table 3  
2D DESSIS simulation results for ideal front or rear side edge isolation for a high-efficiency solar cell structure

Edge isolation type	$V_{\text{oc}}$ (mV)	$J_{\text{sc}}$ (mA/cm <sup>2</sup> )	FF (%)	$\eta$ (%)
From front side	657	37.15	82.7	20.19
From rear side	647	38.80	80.2	20.24

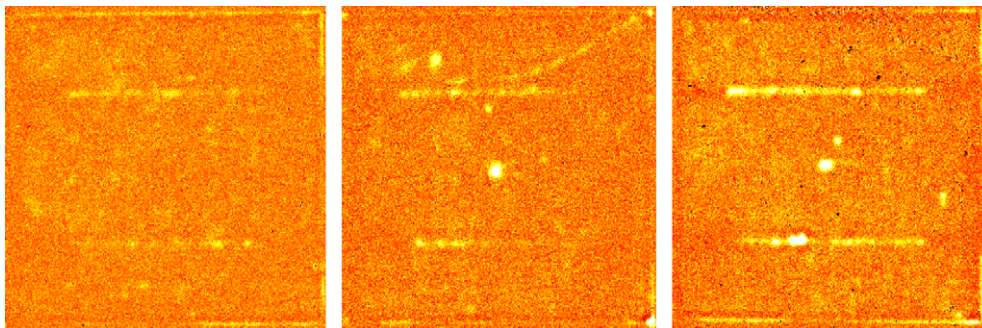


Fig. 4. Dark thermography maps at  $V_{\text{oc}}$  conditions of industrial solar cells of  $156 \times 156 \text{ mm}^2$  size. Left: reference industrial laser edge isolation, middle: edge isolation with waterjet-guided laser (variant 2, cf. Table 1), right: dry UV laser edge isolation.

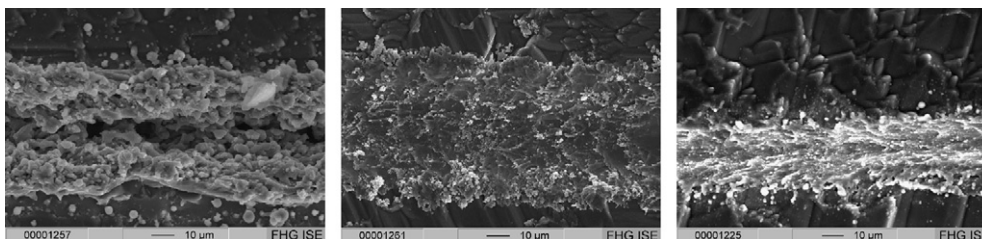


Fig. 5. SEM pictures of laser grooves from different laser processes. Left: reference industrial laser process, middle: waterjet-guided laser (variant 6, cf. Table 1), right: dry UV laser.

These do definitively influence the fill factor but since all measured cells had the same thickness, this mechanical damage must statistically be present on all cells independent of the edge isolation method. Therefore, we expect a decrease in the mean values of the fill factor and efficiency but not an influence of the trend of the mean values.

### 3.4. Suns- $V_{oc}$ measurements

From Suns- $V_{oc}$  measurements on one typical cell of the reference processes, as well as the variants 1 and 6 from Table 1, it was concluded that the absolute fill factor loss due to series resistances was about 5% for all cells. The pseudo fill factors were in the range between 81.3% and 82.0% indicating that no serious recombination problem in the space-charge region existed and there was also no pronounced shunting. Therefore, all laser methods generated satisfying isolation results from the electrical point of view.

### 3.5. Breakage tests and SEM investigation

Another important aspect for the edge isolation process is the mechanical stability of the cells. If significant cracks are introduced in this process step, the wafer has already undergone the complete solar cell process and a breakage in the next steps is the most costly scenario for the cell manufacturer. Additionally, cracks can significantly increase the risk of cell breakage in the module laminating process which can lead to complete module failure. Therefore, the assessment of the mechanical quality of the edge isolation is as important as the study of the electrical performance. In Refs. [16,17], the superior performance of waterjet-guided lasers by reducing the mechanical defects in laser grooving compared to dry lasers was shown.

Analyzing the SEM pictures in Fig. 5, it could be expected that the mechanical properties of the solar cells change with the different edge isolation methods. It was observed that the quality of the dry laser methods was very inhomogeneous over the complete wafer edge, most probably due to wafer thickness variations and associated focusing problems. Therefore, it was quite difficult to depict a representative area. On the other hand, the waterjet-guided laser shows a very homogeneous groove over the entire wafer edge. Less molten and resolidified silicon can be seen in comparison to the dry lasers. This shows that the molten silicon is carried away by the waterjet instead of being redeposited on the cell.

To evaluate quantitatively if the different appearances of the grooves leads to different mechanical stabilities, we performed four line-bending tests of all cells as described in Ref. [14]. The breakage force with its standard deviation has been recorded and summarized in Table 4. For statistical relevance, the number of broken solar cells is not sufficient, so only a first trend can be derived from the experiments. The dry UV laser shows a comparable

Table 4

Breakage forces and respective S.D. of solar cells with edge isolations by different methods

Edge isolation method	Range of breakage force (S.D.) (N)	No. of cells tested
Industrial laser reference	8.8 (4.4)	30
UV dry laser	8.4 (3.3)	10
Waterjet-guided laser	5.0–11.6 (3.6–5.2)	70 (7 for each variant)

breakage force to the industrial reference, while the measured values for the waterjet-guided laser scatter largely. This might be due to the small amount of samples available (seven for each variant compared to 30 samples of the industry reference). Thus, it is difficult to suppress the influence of varying mechanical bulk quality of the cells. But from our studies on wafers [16,17] and the fact that we measured significantly higher breakage forces on some cells, it seems possible to achieve consistently higher breakage forces with further optimization of the waterjet-guided laser edge isolation. To prove this hypothesis, a larger study with more samples and an optimized waterjet-guided laser system is necessary.

## 4. Conclusion

In this paper, we have investigated the effect of guiding a laser beam in a waterjet on the performance of the edge isolation process for industrial multicrystalline silicon solar cells. The experimental study with over 100 solar cells has demonstrated successful edge isolation by waterjet-guided laser. Even with the drawbacks of an IR laser instead of UV, the lack of isolation of the cell's beveled corners and a two to three times larger laser groove, the performance of the reference processes could be obtained. In addition, better second ideality factors have been measured and the groove quality was much more homogeneous than for the dry laser processes.

It can be expected that the edge isolation could be improved further in terms of electrical and mechanical properties by using shorter wavelengths and smaller nozzles. This outlook makes the waterjet-guided laser an interesting option for solar cell microstructuring, not only for edge isolation purposes.

## Acknowledgments

The authors would like to thank Matthias Mesec for performing the edge isolation experiments and Martin Hermle for performing the DESSIS simulations.

## References

- [1] W. Kröniger, D. Perrottet, J.-M. Buchilly, B. Richerzhagen, *Semicond. Packag.* April (2005).

- [2] D. Perrottet, S. Amorosi, B. Richerzhagen, in: Proceedings of the 20th European Photovoltaic Solar Energy Conference, Barcelona, Spain, 2005, p. 877.
- [3] F. Delahaye, M. Löhmann, M. Bauer, G. Vilsmeier, I. Melnyk, A. Hauser, C. Gerhards, M. Krause, S. Lust, H. Nußbaumer, W. Joos, in: Proceedings of the 19th European Photovoltaic Solar Energy Conference, Paris, France, 2004, p. 416–418.
- [4] A. Hauser, G. Hahn, M. Spiegel, H. Feist, O. Breitenstein, J.P. Rakotoniaina, P. Fath, E. Bucher, in: Proceedings of the 17th European Photovoltaic Solar Energy Conference, Munich, Germany, 2001, pp. 1739–1742.
- [5] E. Schneiderlöchner, D.H. Neuhaus, F. Schitthelm, D. Hubatsch, R. Lüdemann, in: Proceedings of the 21st European Photovoltaic Solar Energy Conference, Dresden, Germany, 2006, pp. 923–925.
- [6] G. Emanuel, E. Schneiderlöchner, J. Stollhof, J. Gentischer, R. Preu, R. Lüdemann, in: Proceedings of the 17th European Photovoltaic Solar Energy Conference, Munich, Germany, 2001, pp. 1578–1581.
- [7] R. Preu, G. Emanuel, H. Schmidhuber, D. Biro, C. Voyer, W. Wolke, E. Schneiderlöchner, D. Untiedt, S. Klappert, in: Proceedings of the 19th European Photovoltaic Solar Energy Conference, Paris, France, 2004, pp. 978–981.
- [8] J. Rentsch, F. Binaie, C. Schetter, R. Preu, H. Schlemm, K. Roth, D. Theirich, in: Proceedings of the 19th European Photovoltaic Solar Energy Conference, Paris, France, 2004, pp. 891–894.
- [9] S. Klein, A. Kübelbeck, W. Stockum, in: PV in Europe—From PV Technology to Energy Solutions, Rome, Italy, 2002, pp. 372–374.
- [10] W. Liang, Future Fab International, vol. 19, 2005.
- [11] L. Mayor, Global Semiconductor, vol. 1, 2003.
- [12] O. Breitenstein, J.P. Rakotoniaina, M. Kaes, S. Seren, T. Pernau, G. Hahn, W. Warta, J. Isenberg, in: Proceedings of the 20th European Photovoltaic Solar Energy Conference, Barcelona, Spain, 2005, p. 590.
- [13] R.A. Sinton, A. Cuevas, in: Proceedings of the 16th European Photovoltaic Solar Energy Conference, Glasgow, UK, 2000, pp. 1152–1155.
- [14] D. Kray, H. Kampwerth, E. Schneiderlöchner, A. Grohe, F.J. Kamerewerd, A. Leimenstoll, D. Osswald, E. Schäffer, S. Seitz, S. Wassie, S.W. Glunz, G. Willeke, in: Proceedings of the 19th European Photovoltaic Solar Energy Conference, Paris, France, 2004, pp. 608–611.
- [15] E. Schneiderlöchner, Laserstrahlverfahren zur Fertigung kristalliner Silizium-Solarzellen, Ph.D. Thesis, Institute for Applied Sciences, University of Freiburg, 2004.
- [16] S. Baumann, D. Kray, K. Mayer, A. Eyer, G.P. Willeke, in: Proceedings of the Fourth World Conference on Photovoltaic Energy Conversion, Waikoloa, HI, USA, 2006, pp. 1142–1145.
- [17] S. Schönfelder, J. Bagdahn, S. Baumann, D. Kray, K. Mayer, G.P. Willeke, M. Becker, S. Christiansen, in: Proceedings of the 21st European Photovoltaic Solar Energy Conference, Dresden, Germany, 2006, pp. 588–591.